Enhancing hyperspectral data throughput utilizing wavelet-based fingerprints

Lori M. Bruce[a] and Jiang Li[a]

[a]University of Nevada, Las Vegas, Nevada, USA
in collaboration with the
Department of Energy, Remote Sensing Laboratory, Las Vegas, Nevada, USA

ABSTRACT

Multiresolutional decompositions known as spectral fingerprints are often used to extract spectral features from multispectral/ hyperspectral data. In this study, we investigate the use of wavelet-based algorithms for generating spectral fingerprints. The wavelet-based algorithms are compared to the currently used method, traditional convolution with first-derivative Gaussian filters. The comparison analyses consists of two parts: (a) the computational expense of the new method is compared with the computational costs of the current method and (b) the outputs of the wavelet-based methods are compared with those of the current method to determine any practical differences in the resulting spectral fingerprints. The results show that the wavelet-based algorithms can greatly reduce the computational expense of generating spectral fingerprints, while practically no differences exist in the resulting fingerprints. The analysis is conducted on a database of hyperspectral signatures, namely, Hyperspectral Digital Image Collection Experiment (HYDICE) signatures. The reduction in computational expense is by a factor of about 30, and the average Euclidean distance between resulting fingerprints is on the order of 0.02.

Keywords: wavelet, algorithm, feature extraction, multiresolution, hyperspectral, computational expense

1. INTRODUCTION

Spectral features are often extracted from multispectral/hyperspectral data using a multiresolutional decomposition known as the spectral fingerprint. The spectral fingerprint can be used to provide features that are compact, quantitative, and hierarchical.[1] The method can be used to extract subtle features that are not readily detected visually, and these features have been shown to be useful in separating major atmospheric radiance features from ground (or near-ground) surface radiance features.[1-3] While the spectral fingerprint method has proven to be quite powerful, it has also shown several shortcomings: (a) its implementation requires multiple convolutions with Gaussian filters that are computationally expensive, (b) it requires a truncation of the filter impulse response that can cause spurious errors, and (c) it provides information about the sizes and areas of radiance features but not the shapes. It is proposed that a wavelet-based spectral fingerprint can overcome these shortcomings while maintaining the advantages of the traditional method. Possible benefits of a wavelet-based method include (a) its computational expense may be greatly reduced as compared to current methods; (b) it may be capable of discriminating between various reflectance surfaces; and (c) it may lead to an optimized data compression scheme.

In this study, the authors investigated various methods, wavelet-based and traditional techniques, for computing spectral fingerprints. The computational methods were implemented and applied to hyperspectral images. The images were obtained from airborne hyperspectral remote sensors, namely, the HYDICE. The computational methods were compared in two ways: (a) in terms of computational expense and (b) in terms of final output. For item (a), the computational expense of currently used methods and new wavelet-based methods were analytically determined. Furthermore, both methods were benchmarked for various state-of-the-art systems when applied to hyperspectral data. For item (b), the various methods' outputs, spectral fingerprints, were compared. Metrics, such as signal-to-noise ratios and cross correlations, were used to determine and analyze any differences that might exist between the traditional and wavelet-based outputs.

2. MULTIRESOLUTIONAL DECOMPOSITION AND FEATURE EXTRACTION

For this study, the authors constructed a database of 100 hyperspectral signatures. The database was drawn from a set of four HYDICE image cubes, provided by the Spectral Information Technology Applications Center. Each data cube is (320 pixels) $\times$ (320 pixels) $\times$ (210 spectral channels). Figure 1 illustrates the data cube and the generation of the hyperspectral signature.

For each of the four data cubes, 25 signatures were randomly selected. The signatures were determined randomly by using a two-dimensional, uniform distribution of dimensions 320×320:

$$u(x, y) = \begin{cases} 1/320^2 & \text{for } 0 < x, y < 320 \\ 0 & \text{otherwise} \end{cases} \tag{1}$$

For each data cube, 25 points were drawn from the uniform distribution, and the coordinates within the distribution were used as the coordinates of the signature within the hyperspectral cube.

2.1. Traditional methods

Traditional methods for computing spectral fingerprints require multiple convolutions with Gaussian filters.[1,3] This can be represented mathematically by letting $f(x)$ denote a hyperspectral curve and $G_s(y)$ denote a zero-mean Gaussian filter with standard deviation $s > 0$:

$$G_s(y) = \frac{1}{\sqrt{2\pi}s} \exp\left(-y^2 / 2s^2 \right) \tag{2}$$

The convolution

$$F(x, s) = (f * G_s)(x) = \int_{-\infty}^{\infty} f(x - y) G_s(y) dy \tag{3}$$

produces the smoothing of $f(x)$. Smoothing progresses as s increases. The symbol s is called the scale, and $F(x, s)$ is the scale-space image.[4] Typically, a spectral feature refers to a hill or valley contained between two adjacent inflection points. A scale-space contour refers to an image of the inflection points of the filtered curve for varying scales. As the scale increases, the number of inflection points decreases. As a result, contours usually appear as an assemblage of closed arches, each corresponding to a spectral feature of the curve.[5] When this technique is applied to hyperspectral curves, the characteristic shape of the contours leads to the nickname of "spectral fingerprints." The exact locations of the arch closures and the rate at which they close can provide important information about the spectral features.

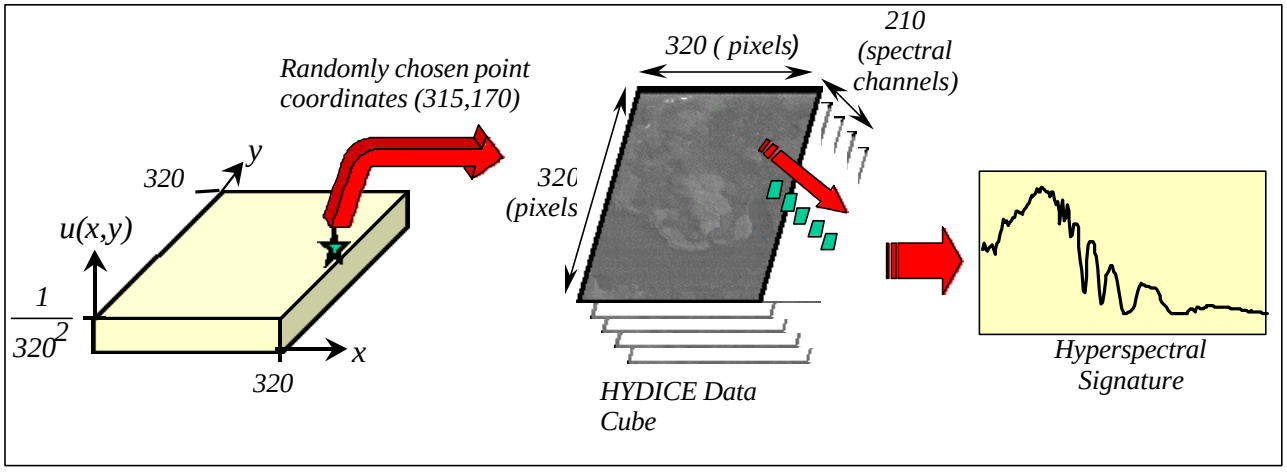

Figure 1. Construction of hyperspectral signature database.

In order to locate the inflection points, it is typical to use first-derivative or second-derivative Gaussian filters. This stems from the fact that when one convolves a first-derivative Gaussian filter with a hyperspectral signature, inflection points will produce extrema in the output curve (or spectral fingerprint). The extrema are tracked across the varying scales, and a plot of the extrema forms the spectral fingerprint. If a second-derivative Gaussian filter is used, the inflection points will produce zero-crossings in the output curve. Either way, the resulting spectral fingerprints are theoretically identical. For this research, the first-derivative Gaussian filter is utilized. The scale-space image is computed by direct convolution. Figure 2 provides an example of a scale-space image and spectral fingerprint for an extracted hyperspectral signature. Figure 3 shows the results of using the traditional convolution method at scales 1 through 8, where the first-derivative Gaussian filter has been used.

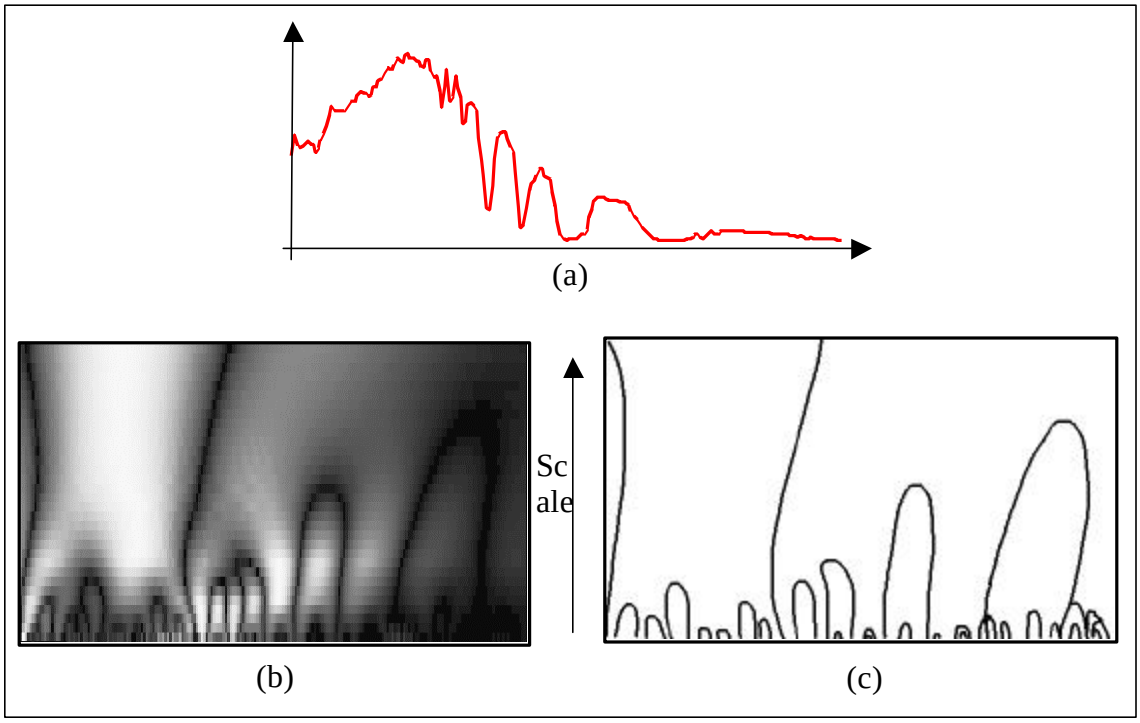

Figure 2. (a) Example hyperspectral signature, (b) scale-space image using first-derivative Gaussian filter, and (c) spectral fingerprint.

2.2. Wavelet-based methods

The scale-space image can be easily computed using wavelet transforms.[5-7] The continuous wavelet transform (CWT) can be defined as the following convolution:

$$W_s f(x) = f(x) * y_s(x) = f(x) * \frac{1}{s} y\left(\frac{x}{s}\right) \tag{4}$$

where s is the scale and $y_s(x)$ is the scaled or dilated wavelet function. It is easy to see that if the wavelet function is the first-derivative Gaussian function, this equation is identical to the traditional scale-space image implementation previously described. When the mother wavelet (scale s = 1) has a variance of σ^2, the scale factor s is equivalent to the standard deviation of the Gaussian function. Note that certain mathematical restrictions apply to the choice of wavelet function, and the first-derivative Gaussian functions satisfy those restrictions.

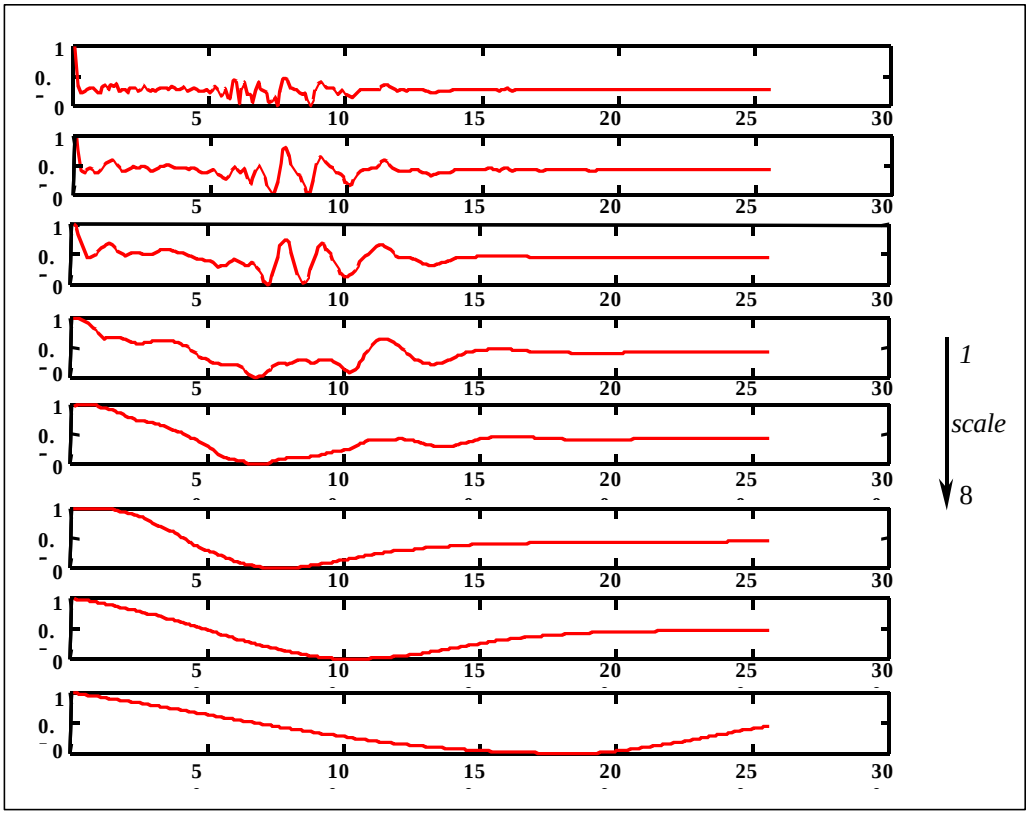

Figure 3. Results of traditional methods – direct convolution with Gaussian filters.

Fast algorithms can be used for computing the wavelet transform in order to avoid the computational expense of direct convolution. One such algorithm is described by Mallat and Zhong.[7] It can be used for computing a discrete-wavelet transform that uses dyadic scales (for integers *k*). For this algorithm, the wavelet function is characterized by two discrete filters, *H* and *G*. The notation H_k and G_k denote the upsampling of filters *H* and *G* by the factor of 2^k. The following algorithm computes the discrete-wavelet transform, $W_{2^{k+1}} f(x)$, at scale $s = 2^{k+1}$ of the input signature $f(x)$:

$k = 0$

$S_{2^k} f(x) = f(x)$

while $(k < K)$

$$W_{2^{k+1}} f(x) = \frac{1}{l_k} \cdot S_{2^k} f(x) * G_k$$

$$S_{2^{k+1}} f(x) = S_{2^k} f(x) * H_k$$

$k = k + 1$

end of while.

The computation of the wavelet transform is an iterative process where the input signature is decomposed into approximation and detail signals. At each iteration, the approximation is then further decomposed into coarser approximation and detail signals. For example, at each scale 2^k the current approximation signal, $S_{2^k} f(x)$, is decomposed into the next higher-scale

approximation signal, $S_{2^{k+1}} f(x)$, and a detail signal, $W_{2^{k+1}} f(x)$. Due to discretization, the wavelet extrema corresponding to an inflection point in the original spectral curve do not have the same amplitude at all scales as they should in the continuous model. The coefficients l_k compensate for this discrete effect, and they correspond to the filters *H* and *G*. To avoid discontinuities at the boundaries, the endpoints of the original spectral curve are extended using mirror reflections. Figure 4 provides an example of the application of this method to an extracted hyperspectral curve.

3. COMPUTATIONAL EFFICIENCY ANALYSIS

The computational efficiency analysis of the radiance fingerprint methods can be divided into two portions: (a) the analytical assessment and (b) the experimental benchmarking. Two algorithms, the direct convolution with the first-derivative Gaussian filter and the Mallat/Zhong wavelet algorithm, were analyzed. For thoroughness, two other wavelet methods were analytically assessed. These included a standard CWT algorithm and a fast algorithm for computing the CWT at integer scales.

3.1. Computational expense—analytical assessment

The order of complexity for direct convolution is

$$O_d = O(N \sum_{s=1}^{P} s) \tag{5}$$

where *N* is the number of samples in the original spectral curve and *P* is the total number of scales utilized. At each scale, *s*, a direct convolution must be performed. Let *L* be the length of the original, first-derivative Gaussian filter. At the first scale, the operations required are (*L* multiples per sample of the spectral curve) and *((L-1)* additions per sample of the spectral curve). Therefore for the first scale, a constant of *(C=2L-1)* operations must be performed per sample. At each scale, the filters are dilated by the scaling factor *s*, or s. Thus, the length of the Gaussian filter becomes $L \cdot s$. At scale *s*, the number of operations per sample is *(2Ls - 1),* which becomes *(2Ls)* for very large scales. Thus, the number of operations per scale is *(2LsN).* For the total *P* scales, the number of operations must be summed, such that the number of operations becomes

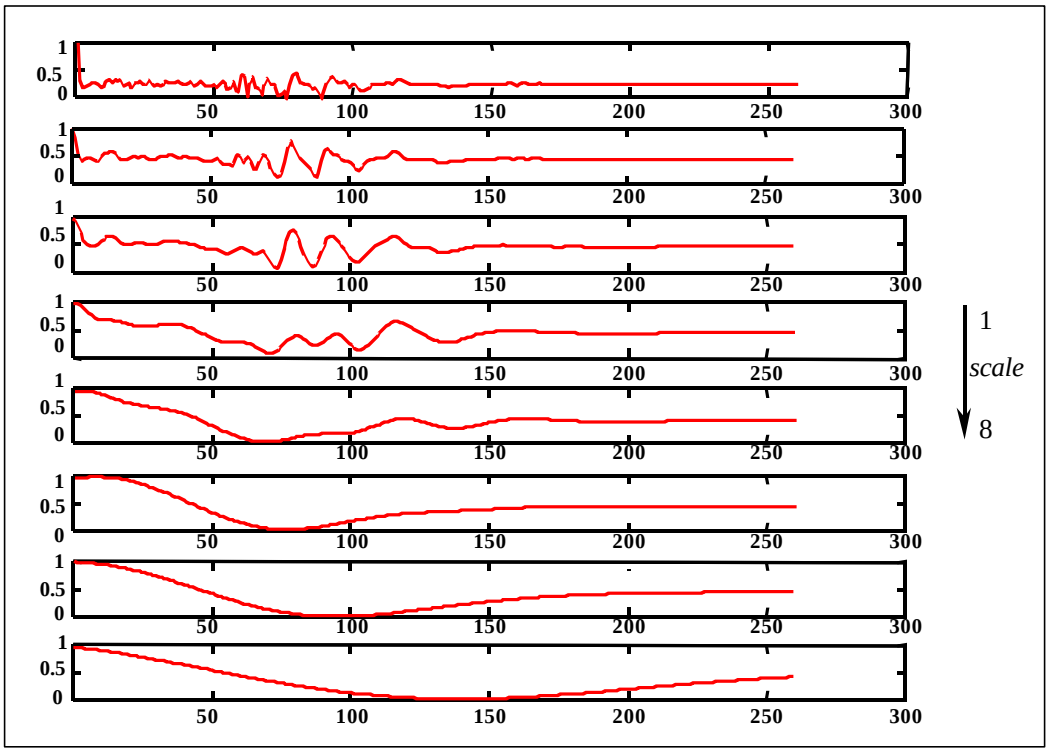

Figure 4. Results of wavelet-based method – Mallat/Zhong algorithm.

$$(2LN\sum_{s=1}^{P} s) \tag{6}$$

The term (2*L*) is a constant, and thus the order of complexity becomes O_d.

The order of complexity for the Mallat/Zhong wavelet algorithm is $O_{MZ}=O(N\log N)$, where *N* is the number of samples in the original spectral curve. This is *O(N)* per scale with a total of *log(N)* possible scales. At each scale, a direct convolution must be performed to compute the wavelet transform, $W_{2^{k+1}} f(x)$, and a direct convolution must be performed to compute the approximation signal, $S_{2^{k+1}} f(x)$. Let the length of the original spectral curve be *N*, the length of the original filter *G* be *L*, and the length of the original filter *H* be *M*. At the first scale, the operations required are $L + M$ multiples per sample of the spectral curve and $(L - 1) + (M - 1)$ additions per sample of the spectral curve. Therefore for the first scale, a constant of $(C=2L+2M-2)$ operations must be performed per sample. At each scale, the filters are upsampled by a factor of 2^p. This introduces 2^p-1 zeros between each sample of the filters, which theoretically would increase the lengths *L* and *M* at each scale. However, the algorithm can be implemented in an intelligent way so as to avoid the multiples/additions with the zero-samples of the filters. For example, when implementing this algorithm on a DSP chip, one would use an indirect addressing mode indexed by the amount of upsampling at each scale. In this way, the order of complexity is independent of the scale. Thus for each scale, the order of complexity is (CN), or *O(N)*. Since this method uses dyadic scales, the total number of utilized scales is $\log_2 N$. As a result, the total order of complexity is $O(N\log N)$.

For a standard CWT without the use of filter banks, the order of complexity is the same as for the direct convolution of a first-derivative Gaussian filter

$$O_{cwt}=O(N\sum_{s=1}^{P} s) \tag{7}$$

where *N* is the number of samples in the original spectral curve and *P* is the total number of scales utilized. This stems from the discussion in Section 2 about the similarities between the direct convolution and the CWT. At each scale, *s*, a direct convolution must be performed. Let *L* be the length of the original wavelet function. At the first scale, the operations required are *L* multiples per sample of the spectral curve and $(L - 1)$ additions/sample of the spectral curve. Therefore for the first scale, a constant of $(C = 2L - 1)$ operations must be performed per sample. At each scale, the wavelet functions are dilated by the scaling factor *s*. Thus, the length of the wavelet function becomes $L \cdot s$. At scale *s*, the number of operations per sample is $(2Ls - 1)$, which becomes $(2Ls)$ for very large scales. Thus, the number of operations per scale is $(2LsN)$. For the total *P* scales, the number of operations must be summed such that the number of operations becomes

$$(2LN\sum_{s=1}^{P} s) \tag{8}$$

The term (2*L*) is a constant, and thus the order of complexity becomes $O_{cwt} = O_d$.

A fast algorithm for the computation of the CWT at integer scales was also analyzed.[8] The algorithm was developed by Unser and Aldroubi, and the order of complexity was found to be $O_{UA} = O(N)$. The algorithm utilizes polynomial spline functions for the wavelet functions. The spline functions can easily be used to approximate the first-derivative Gaussian filter. The algorithm consists of three steps: (a) initialization, (b) iterated moving sum, and (c) zero-padded filtering. One can go through these three steps and calculate the number of multiples and additions required per scale. The number of multiples required is $(n_s/2)$, where n_s is the length of the kernel representing the B-spline coefficients of the wavelet function, $y(x)$, that have been upsampled by a factor of *s*, the integer scale. The number of additions required is $(2n + n_s + 1)$, where *n* is the degree of the spline function representing the wavelet function, $y(x)$. The number of total operations per scale is then $((2n + \frac{3}{2} n_s + 1)\cdot N)$. Thus, the order of complexity per scale is *O(N)*. If we use this algorithm at dyadic scales, the order of complexity is equivalent to that of the Mallat/Zhong algorithm, $O_{UA} = O_{MZ} = O(N\log N)$. However, since this algorithm allows for fast computation of the wavelet transform at integer scales, we are not restricted to dyadic scales. This could be of importance when extracting spectral features from the spectral fingerprint. In general, the spectral fingerprint could be

computed at dyadic scales, but when important spectral content is detected, the integer-scale algorithm could then be used to compute the spectral fingerprint over a more continuous range of scales.

3.2. Computational expense—experimental assessment

The experimental determination of the computational expense of the spectral fingerprint methods was completed by computing the number of floating-point operations during the computation of the scalar decompositions, or scale space images. Note that the Mallat/Zhong algorithm could be implemented in such a way that the zero-multiples are not computed. Thus a special program was written to compute the total number of the floating-point operations. As a result, for the method of the direct convolution with Gaussian filters, approximately the total number of addition operations, with respect to a total of *log(N)* possible scales, was (386,325), and the total number of multiply operations, with respect to a total of *log(N)* possible scales, was (390,144). Similarly, for the Mallat/Zhong algorithm, there were approximately a total of (10,901) addition operations and a total of (18,776) multiply operations, corresponding to a total of *log(N)* possible scales. For a practical view of the difference of the computational expense between the traditional method and the Mallat/Zhong wavelet method, typical microprocessor chips were chosen to evaluate the computational efficiency based on the criteria of time costs. For DSP56002 and TMS320C30 chips, it takes 60ns to implement a floating-point addition or a floating-point multiply. For 333MHz Pentium II and 333 MHz UltraSPARC-IIi chips, it takes 3ns to finish a floating-point addition or a floating-point multiple. Table 1 shows some experimental results of the computational expense, and Figure 5 illustrates the contrast of the computational efficiency.

Table 1. Experimental results of computational expense

		"Traditional" method		Wavelet-based method	
		386,325 adds	390,144 muls	10,901 adds	18,766 muls
DSP56002	60 ns/add 60 ns/mul	46.59 ms		1.78 ms	
TMS320C30	60 ns/add 60 ns/mul	46.59 ms		1.78 ms	
333 MHz Pentium II	3 ns/add 3 ns/mul	2.33 ms		0.09 ms	
333 MHz UltraSPARC-IIi	3 ns/add 3 ns/mul	2.33 ms		0.09 ms	

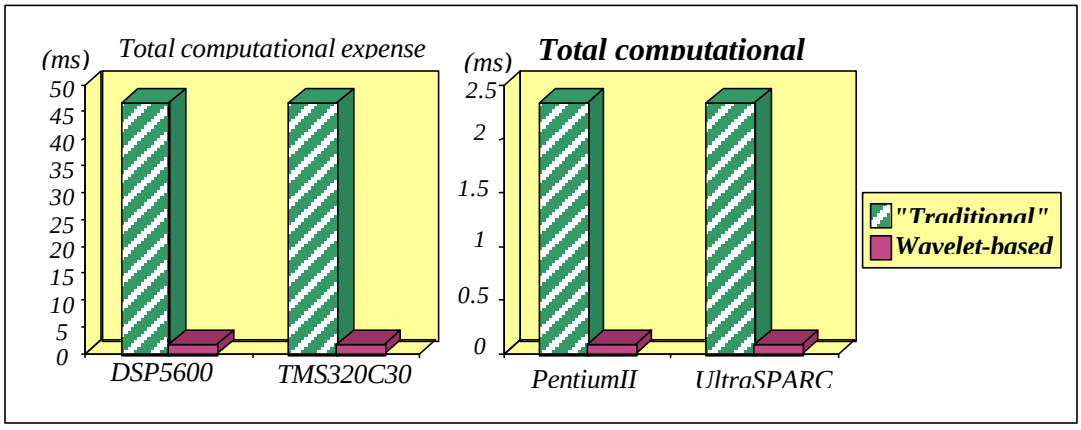

Figure 5. Experimental assessment of computational efficiency.

4. COMPARISON ANALYSIS OF TRADITIONAL AND WAVELET-BASED METHODS

Various methods were implemented for comparing the outputs of the algorithms. These methods were designed to determine and analyze any differences that might exist between the methods' resulting spectral fingerprints. The two algorithms being compared were the traditional, first-derivative Gaussian-filtering method and the Mallat/Zhong algorithm. The methods for

comparison included normalized cross correlation and normalized Euclidean distance measures. The comparison was performed at each level of the decomposition (each scale of the scale-space image). The comparison analysis was not conducted on the actual spectral fingerprint. In order to create a spectral fingerprint from the scale-space image, the maxima (or zero-crossings) of the image must be tracked across the varying scales. The technique used to go from the scale-space image to the spectral fingerprint is the same regardless of the method used to obtain the scale-space image. Furthermore, in most spectral fingerprints only the maxima (or zero-crossings) are retained; *i.e.*, the fingerprint is a plot of the maxima (or zero-crossings) locations. By comparing the outputs of the two methods before converting to a fingerprint, a more conservative measurement of the errors will be made.

The normalized cross correlation at each scale is defined as

$$j(x) = \frac{1}{E} \sum_{y=-\infty}^{\infty} T(y) W(y + x) \tag{9}$$

where

$$E = \sqrt{\sum_i (T_i)^2} \sqrt{\sum_i (W_i)^2} \tag{10}$$

T is the traditional Gaussian-filtered signal and W is the result of the Mallat/Zhong wavelet algorithm. Note that if the two signals are identical, $j(0) = 1$. If the two signals are identical except for a linear shift by k samples, $T(y) = W(y + k)$, then $j(k) = 1$. For this research, the entire cross correlation is computed, and the maximum value and its shift, k, is recorded. Figure 6 shows a plot of the maximum cross correlation values for various scales; the results are for a hyperspectral signature selected at random from the database of 100 signatures.

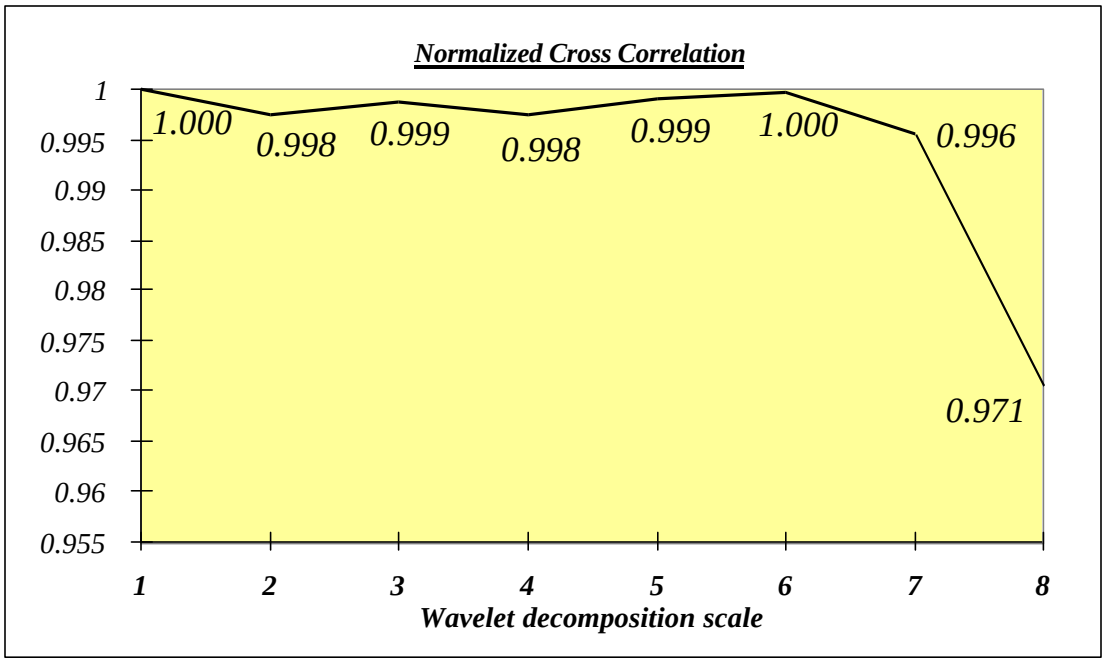

Figure 6. Normalized cross correlation maxima for hyperspectral curve.

One can view the scale-space image as a collection of vectors, one for each scale. As a result, vectorial distances can be used to measure the difference between the results of the two methods. For this study, a normalized Euclidean distance measure is utilized to compare the outputs of the two methods at each scale. This measure is defined as

$$Eucl = \frac{\sqrt{\sum_i (T_i - W_i)^2}}{\sqrt{\sum_i (T_i^2)}\sqrt{\sum_i (W_i^2)}}, \tag{11}$$

where T is the traditional Gaussian-filtered signal and W is the result of the Mallat/Zhong wavelet algorithm. The Euclidean distance is measured for each scale. Furthermore, it is computed for various linear shifts in W. Thus, it is similar to the normalized cross correlation, except that the Euclidean distance is minimized to zero when the two methods produce identical results. Figure 7 shows an example plot of the minimum Euclidean distances for various scales; the results are for a hyperspectral signature selected at random from the database of 100 signatures.

For this study, the error measures discussed in the above paragraphs were applied to the 100 hyperspectral signatures in our database. For each error measure, the mean, m, and variance, s^2, of the 100 errors were computed. The resulting means and variances are listed in Table 2, where m_{Corr} and s^2_{Corr} refer to the normalized cross correlation mean and variance, respectively. Likewise, m_{Euc} and s^2_{Euc} refer to the normalized Euclidean distance mean and variance, respectively. It can be seen that relatively little error is induced by using the Mallat/Zhong algorithm while the computational expense is greatly reduced.

Table 2. Error analysis for 100 randomly extracted hyperspectral signatures

Scale	m_{Corr}	s^2_{Corr} $(\times 10^{-3})$	m_{Euc}	s^2_{Euc} $(\times 10^{-3})$
1	1.0000	0.0000	0.0000	0.0000
2	0.9966	0.0061	0.0263	0.5183
3	0.9986	0.0002	0.0120	0.0546
4	0.9972	0.0023	0.0155	0.0636
5	0.9984	0.0013	0.0111	0.0259
6	0.9984	0.0021	0.0081	0.0206
7	0.9945	0.0080	0.0154	0.0198
8	0.9641	0.2088	0.0382	0.0438
Average	0.9935	0.0286	0.0157	0.0997

5. CONCLUSIONS

The results of this preliminary study indicated that a wavelet-based method is feasible and practical for the analysis of hyperspectral imagery through the radiance fingerprint. Furthermore, the results indicated that wavelet-based methods can be computationally efficient as compared to traditional, first-derivative Gaussian-filtering methods. From the experimental assessment of the two methods, it was clear that the computational expense was greatly reduced. Utilizing the Mallat/Zhong wavelet-based method, the computational expense was reduced by a factor of about 26. This conclusion also coincided with the result of the analytical assessment, where the reduction was by a factor of about 30. In this research, the number of sampling points of each hyperspectral signature was 210, since HYDICE data were used. When using dyadic scales for the wavelet-based method, the total number of utilized scales was 8. If the signatures were longer (more spectral channels), the number of utilized scales would increase. With an increase in scales, the computational efficiency gained from using the wavelet-based algorithms would also increase.

The final outputs (spectral fingerprints) of the traditional and the Mallat/Zhong wavelet-based methods were compared. This was to ensure that the "fast" algorithms did not cause any major errors in the spectral fingerprints. The outputs of the two methods were compared at each scale and across all scales. The comparison was conducted using normalized cross-

correlations and normalized Euclidean distances. It was concluded that some differences exist between the traditional, first-derivative Gaussian-filtering method and the Mallat/Zhong algorithm; however, the induced errors were relatively small. While a small error was induced, the computational expense was greatly reduced.

Future research in this area includes the use of wavelet-based features extraction from the hyperspectral signatures. With the use of the wavelet-based algorithms, spectral features can be extracted by the modulus-maximus method. These can quantify the magnitude, variance, location, and Lipschitz order of spectral features within the signatures. These features are being investigated for their ability to discriminate between classes of critical signatures.

6. ACKNOWLEDGEMENTS

This work was supported by the U.S. Department of Energy, Nevada Operations Office, under contract No. DE-AC08-96NV11718. By acceptance of this article, No. DOE/NV/11718--366, the publisher and/or recipient acknowledge the right of the U.S. government to retain a nonexclusive, royalty-free license in and to any copyright covering the article.

7. REFERENCES

1. M. A. Piech and K. R. Piech, "Fingerprints and Fractal Terrain," *Mathematical Geology*, vol. 22, no. 4, pp. 457-485, 1990.
2. James B. Campbell, *Introduction to remote sensing*, 2nd Ed., Guilford Press, 1996.
3. R. A. Schowengerdt, *Remote Sensing: Models and Methods for Image Processing*, 2nd Ed., Academic Press, 1997.
4. A. Witkin, "Scale Space Filtering," *Proc. Int. Joint Conf. Artif. Intell.*, pp. 1019-1022, 1983.
5. L. M. Bruce, "Isolation Criteria for the Wavelet Transform Mod-Max Method", *IEEE Trans Circuits and Systems II*, vol. 45, no. 8, pp. 1084-1087, 1998.
6. S. Mallat, *A wavelet tour of signal processing*, Academic Press, 1998.
7. S. Mallat and S. Zhong, "Characterization of Signals from Multiscale Edges," *IEEE Trans. Patt. Anal. Machine Intell.*, vol. 14, no. 7, pp. 710-732.
8. M. Unser, A. Aldroubi, and S.J. Schiff, "Fast Implementation of the Continuous Wavelet Transform with Integer Scales," *IEEE Trans. Signal Processing*, vol. 42, no. 12, pp. 3519-3523, 1994.

DISTRIBUTION

DOE Public Reading Facility	(1)
OSTI	(2)
TIRC	(1)